

Tailoring single-ion magnet properties of coordination polymer $C_{11}H_{18}DyN_3O_9$ (Dy-CP) using Radial Effective Charge model (RECM) and Superposition model (SPM)

Dinabandhu Halder,^a Yatramohan Jana,^{a,*} Danuta Piwowarska,^b Paweł Gnutek^b and Czesław Rudowicz^c

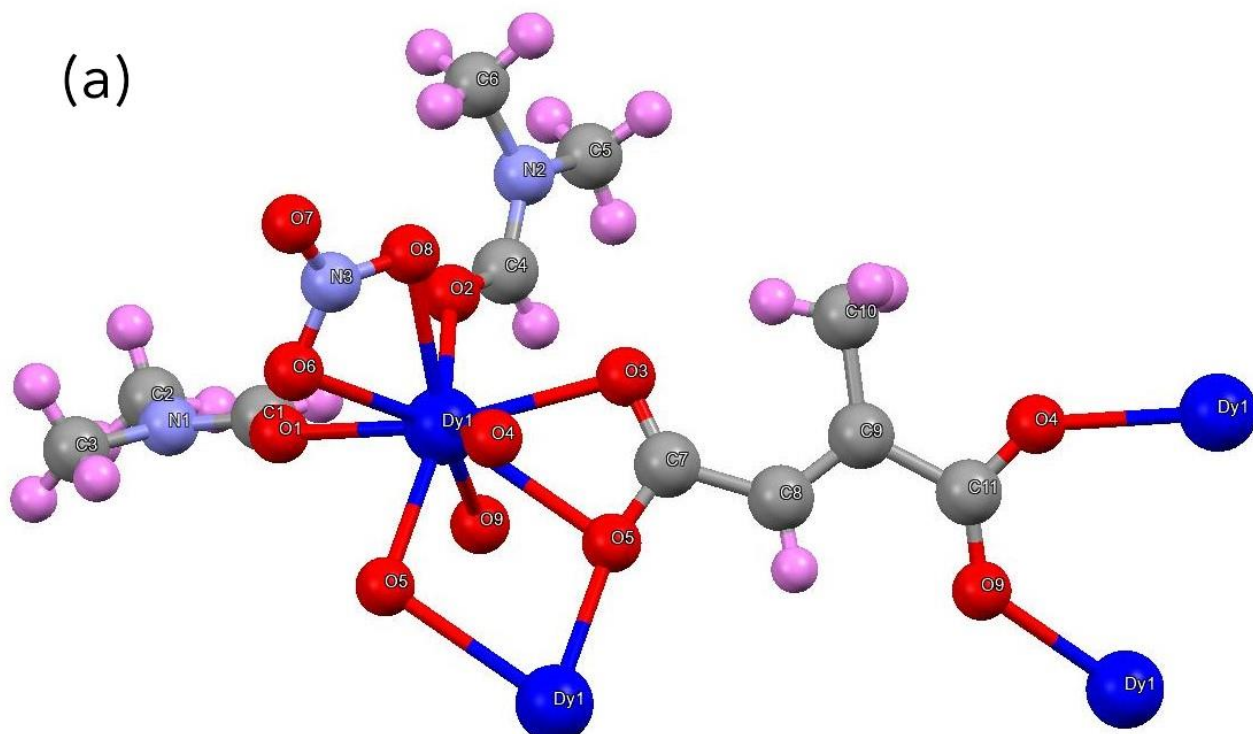
^aDepartment of Physics, University of Kalyani, Kalyani -741235, Nadia, W.B., India

^bFaculty of Mechanical Engineering and Mechatronics, West Pomeranian University of Technology in Szczecin, 70-311 Szczecin, Poland

^cFaculty of Chemistry, Adam Mickiewicz University, 61-614 Poznań, Poland

S1. Crystal structure of $C_{11}H_{18}DyN_3O_9$ (Dy-CP)

The Dy-based coordination polymer $C_{11}H_{18}DyN_3O_9$ (Dy-CP) crystallizes in a monoclinic space group $P2_1/c$ (C_{2h}^5 : no. 14) with a distorted tricapped triangular prismatic geometry.¹ Lattice parameters are: $a = 11.8534 \text{ \AA}$, $b = 11.8871 \text{ \AA}$, $c = 12.5771 \text{ \AA}$ and $\beta = 104.182^\circ$. The unit cell contains four formula units, i.e., $Z = 4$ and all atoms reside at 4e Wyckoff sites, having triclinic (C_1) site symmetry. Each Dy^{3+} at triclinic C_1 site is coordinated to nine oxygen ligands bound to different chemical groups: two oxygens, O1 and O2, containing monodentate dimethylformamide (DMF) molecules; three monodentate oxygens, O3, O4 and O9; two bridging oxygens, O5 and O5', with neighbouring Dy; and two oxygens, O6 and O8, containing bidentate bridging nitrate ion (Fig. S1(a)). Two Dy^{3+} ions interact via two carboxylate oxygen atoms. The atomic coordinates of Dy and oxygen atoms obtained from a CIF data¹ are collected in Table S1. The Dy–O bond lengths vary within the range of 2.26 – 2.65 Å (see Table S2) within [DyO₉] coordination polyhedron (see Fig. S1(b)), while the Dy–Dy bond distances are 7.58, 8.664, 10.455 (in Å) within the conventional unit cell of Dy-CP.



(b)

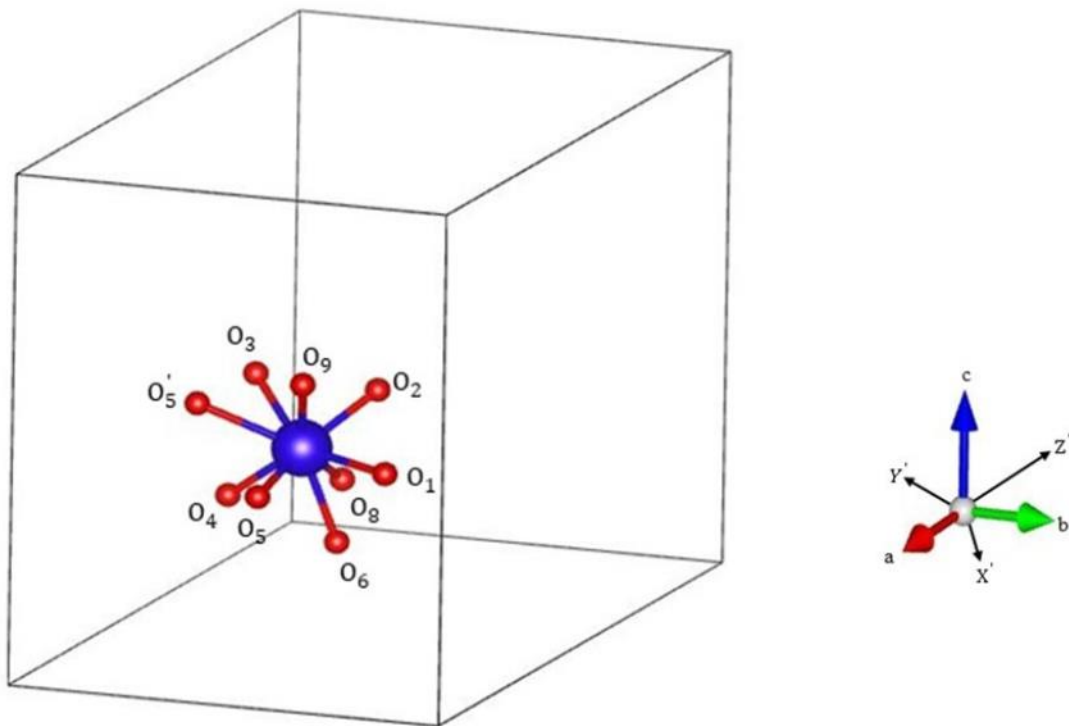


Fig. S1 (a) Crystal structure of $C_{11}H_{18}DyN_3O_9$ (Dy-CP). (b) Left panel: The $[DyO_9]$ polyhedron: Dy ion (blue) coordinated to nine oxygen ions (red) in monoclinic Dy-CP crystal. Right panel: the CAS (a,b,c) and the rotated CAS* (X' , Y' , Z'). For explanations, see text.

Table S1 The atomic coordinates of Dy and oxygen atoms in $[DyO_9]$ polyhedron in Dy-CP compound.¹

Atoms	Atomic coordinates		
	x/a	y/b	z/c
Dy	0.84575	0.57199	0.46070
O ₁	0.85400	0.77070	0.42820
O ₂	0.70290	0.65270	0.53480
O ₃	0.79500	0.42950	0.57930
O ₄	0.85580	0.40890	0.35890
O ₅	1.02170	0.58580	0.42220
O _{5'}	0.97830	0.41420	0.57780
O ₆	0.77890	0.61300	0.25870
O ₈	0.65200	0.54060	0.33480
O ₉	0.96010	0.64620	0.62690

Table S2 The Dy-O bond lengths (r_i), idealized spherical polar coordinates (R_i, θ_i, ϕ_i) in the CAS*, the angles (ϑ_i, φ_i) in the rotated CAS*, and the effective charge of oxygen ligands surrounding Dy atom in Dy-CP that serve as input for SIMPRE calculations. For explanations, see, text.

Oxygen atoms	r_i (Å)	Idealized spherical polar coordinates in					Z_i	
		CAS*			rotated CAS*			
		R_i (Å)	θ_i (°)	ϕ_i (°)	ϑ_i (°)	φ_i (°)		
O ₁	2.4033	1.5033	100.37	87.70	80.86	269.92	-0.212	
O ₂	2.3301	1.4301	54.70	149.7	12.8	212.55	-0.212	
O ₃	2.4281	1.5481	47.54	251.0	71.42	112.0	-0.199	
O ₄	2.3424	1.4424	124.0	273.41	122.1	48.42	-0.199	
O ₅	2.2597	1.3597	116.13	4.64	159.42	254.60	-0.192	
O _{5'}	2.6499	1.7699	65.76	309.10	119.5	128.82	-0.192	
O ₆	2.5167	1.6367	158.81	147.60	96.85	338.0	-0.206	
O ₈	2.4777	1.5977	114.33	189.51	58.4	13.15	-0.206	
O ₉	2.3657	1.4657	42.0	33.87	91.14	195.1	-0.199	

Table S3 The predicted crystal-field parameters (CFPs) in cm^{-1} together with the invariant quantities: the Stevens CFPs/ C_k^q calculated using RECM: (b) in the CAS* and (c) in the rotated CAS*; converted Wybourne CFPs/ B_{kq} : (e) from column (b), (f) from column (c); and (g) SPM/ B_{kq} . The respective CFPs/ B_{kq} after the 3DD and CST standardisation are listed in columns (x/3DD), x = e, f, g. For explanations, see, text.

Stevens CFPs			Wybourne CFPs							
C_k^q			B_{kq}^{\square}						SPM/ B_{kq}	
(a)	(b)	(c)	(d)	(e)	(e/3DD) ¹⁾	(e'/CST)	(f)	(f/3DD) ²⁾	(g)	(g/3DD) ³⁾
C_2^0	8.5	88.7	B_{20}	17.1	-234.0	268.8	177.4	268.8	177.4	270.3
C_2^1	166.5	200.0	B_{21}^r	-68.0	0	0	-81.7	0	-81.5	0
C_2^{-1}	-442.4	208.3	B_{21}^i	-180.6	0	0	85.0	0	86.1	0
C_2^2	30.0	73.1	B_{22}^r	24.5	-124.0	81.3	59.7	81.3	61.0	83.6
C_2^{-2}	-84.3	119.5	B_{22}^i	68.8	0	0	-97.6	0	-100.0	0
			S_2	130.7	130.7	130.7	130.7	130.7	132.0	131.9
C_4^0	-99.0	116.7	B_{40}	-792.0	662.2	59.0	933.8	58.8	933.0	-23.6
C_4^1	-513.8	68.4	B_{41}^r	459.5	-13.1	275.3	-61.2	275.1	40.4	233.2
C_4^{-1}	33.5	-399.8	B_{41}^i	30.0	309.6	-97.1	-357.6	97.6	-358.0	146.0
C_4^2	131.0	-118.5	B_{42}^r	165.7	16.4	397.9	-150.0	398.4	-163.6	442.2
C_4^{-2}	56.6	256.8	B_{42}^i	-71.6	-127.0	535.9	-325.0	-535.3	-332.0	-498.0
C_4^3	337.6	-1138.8	B_{43}^r	-114.1	578.0	31.7	385.0	32.4	386.0	67.3
C_4^{-3}	-1043.3	71.7	B_{43}^i	-352.7	-497.8	578.1	24.2	-578.6	24.5	-592.7
C_4^4	586.7	271.0	B_{44}^r	561.0	-193.4	311.3	259.1	311.0	262.2	323.5
C_4^{-4}	35.0	330.8	B_{44}^i	-33.3	-246.3	-216.6	-316.3	216.7	-321.3	209.1

			S₄	474.1	474.1	474.2	474.1	474.2	477.0	477.0
C_6^0	22.3	20.8	B ₆₀	356.8	-97.5	162.1	332.5	162.0	332.5	111.7
C_6^1	-94.7	138.8	B ₆₁ ^r	117.0	-212.6	-35.1	-171.4	-35.0	-170.6	-15.1
C_6^{-1}	230.2	-177.5	B ₆₁ ⁱ	284.2	-116.5	-56.0	-219.1	56.2	-233.0	58.7
C_6^2	-105.3	-75.2	B ₆₂ ^r	-164.5	-101.4	198.8	-117.4	198.8	-75.3	137.6
C_6^{-2}	56.8	90.7	B ₆₂ ⁱ	-88.6	-183.3	277.3	-141.6	-277.1	-142.0	-296.4
C_6^3	-149.3	167.5	B ₆₃ ^r	116.6	-269.7	83.4	-130.7	84.0	-134.7	91.0
C_6^{-3}	-155.6	255.5	B ₆₃ ⁱ	-121.5	180.2	92.3	199.5	-92.4	134.5	-102.8
C_6^4	59.0	-192.0	B ₆₄ ^r	84.1	-237.3	-168.0	-273.5	-167.3	-275.5	-133.0
C_6^{-4}	-34.2	-25.7	B ₆₄ ⁱ	48.7	205.0	215.7	36.7	-216.0	60.3	-197.1
C_6^5	761.1	-72.3	B ₆₅ ^r	-231.3	-104.1	-278.1	22.0	-277.8	-29.2	-285.5
C_6^{-5}	-507.2	-600.7	B ₆₅ ⁱ	-154.1	43.0	190.4	-182.5	-191.0	-203.0	-230.1
C_6^6	-88.2	-93.7	B ₆₆ ^r	-93.0	105.1	39.3	-98.6	39.3	-131.3	88.5
C_6^{-6}	158.6	36.2	B ₆₆ ⁱ	-167.0	-99.6	73.2	-38.1	-73.2	-76.4	-105.1
			S₆	230.3	230.3	230.3	230.2	230.2	230.5	230.5
			S	313.5			313.5		315.2	

The Euler angles are: ¹⁾ $\alpha = 87.26$, $\beta = 49.17$, $\gamma = -62.63$; ²⁾ $\alpha = 36.81$, $\beta = 32.67$, $\gamma = -12.90$; ³⁾ $\alpha = 36.90$, $\beta = 32.98$, $\gamma = -12.98$ (all in degree).

Table S4 The calculated low-lying electronic energy (E_i) levels in cm^{-1} within the ground multiplet ${}^6\text{H}_{15/2}$ and associated wave functions (Ψ_i) of Dy^{3+} ion in Dy-CP: (a) E_i , (b) Ψ_i and (c) g-tensor predicted using Stevens CFPs/ C_k^q calculated using RECM in the rotated CAS* (column c in Table S3); (d) E_i , (e) Ψ_i and (f) g-tensor predicted using the converted Wybourne CFPs/ B_{kq} (column f in Table S3); and (g) E_i using SPM CFPs/ B_{kq} (column g in Table S3). Only the modulus square of each M_j contribution greater than 5% is provided (except for the ground doublet). Barycenter (\bar{E}) of the energy levels in cm^{-1} is also given.

SIMPRE			SPECTRE					
E_i	Ψ_i	g-tensor (g_x , g_y , g_z)	E_i	Ψ_i		g-tensor (g_x , g_y , g_z)	E_i	
(a)	(b)	(c)	(d)	(e)		(f)	(g)	
0.0	$0.87 \mp\frac{15}{2}\rangle + 0.01 \mp\frac{11}{2}\rangle + 0.03 \mp\frac{9}{2}\rangle + 0.02 \mp\frac{7}{2}\rangle + 0.023 \mp\frac{3}{2}\rangle + 0.023 \mp\frac{1}{2}\rangle + 0.013 \pm\frac{1}{2}\rangle + 0.005 \pm\frac{3}{2}\rangle + 0.004 \pm\frac{5}{2}\rangle + 0.002 \pm\frac{7}{2}\rangle + 0.002 \pm\frac{9}{2}\rangle \#$	1.03, 0.28, 18.1	0.0	$0.862 \mp\frac{15}{2}\rangle + 0.01 \mp\frac{11}{2}\rangle + 0.033 \mp\frac{9}{2}\rangle + 0.02 \mp\frac{7}{2}\rangle + 0.02 \mp\frac{3}{2}\rangle + 0.02 \mp\frac{1}{2}\rangle + 0.015 \pm\frac{1}{2}\rangle + 0.003 \pm\frac{3}{2}\rangle + 0.004 \pm\frac{5}{2}\rangle + 0.003 \pm\frac{7}{2}\rangle + 0.01 \pm\frac{15}{2}\rangle$		0.68, 0.36, 17.82	0	
30.7	$0.08 \mp\frac{15}{2}\rangle + 0.26 \mp\frac{3}{2}\rangle + 0.18 \mp\frac{1}{2}\rangle + 0.25 \pm\frac{1}{2}\rangle + 0.08 \pm\frac{5}{2}\rangle$	9.94, 0.34, 2.01	28.4	$0.07 \mp\frac{15}{2}\rangle + 0.26 \mp\frac{3}{2}\rangle + 0.18 \mp\frac{1}{2}\rangle + 0.24 \pm\frac{1}{2}\rangle + 0.10 \pm\frac{5}{2}\rangle$		14.66, 0.57, 1.70	29.6	

74.0	$0.39 \mp\frac{13}{2}\rangle + 0.13 \mp\frac{7}{2}\rangle +$ $0.14 \mp\frac{5}{2}\rangle + 0.11 \mp\frac{3}{2}\rangle +$ $0.08 \pm\frac{1}{2}\rangle$	2.50, 4.50, 9.15	69.3	$0.20 \mp\frac{13}{2}\rangle + 0.05 \mp\frac{9}{2}\rangle +$ $0.11 \mp\frac{7}{2}\rangle + 0.15 \mp\frac{5}{2}\rangle +$ $0.06 \pm\frac{1}{2}\rangle + 0.11 \pm\frac{3}{2}\rangle +$ $0.15 \pm\frac{13}{2}\rangle$	1.90, 9.27, 2.91	70.6
104.6	$0.32 \mp\frac{13}{2}\rangle + 0.11 \mp\frac{11}{2}\rangle +$ $0.08 \mp\frac{9}{2}\rangle + 0.14 \mp\frac{5}{2}\rangle +$ $0.07 \pm\frac{1}{2}\rangle + 0.07 \pm\frac{3}{2}\rangle$	6.88, 4.31, 8.68	99.5	$0.21 \mp\frac{13}{2}\rangle + 0.06 \mp\frac{9}{2}\rangle +$ $0.05 \mp\frac{7}{2}\rangle + 0.1 \mp\frac{3}{2}\rangle +$ $0.06 \pm\frac{1}{2}\rangle + 0.13 \pm\frac{5}{2}\rangle +$ $0.12 \pm\frac{11}{2}\rangle + 0.14 \pm\frac{13}{2}\rangle$	8.26, 3.25, 0.87	99.4
166.4	$0.09 \mp\frac{13}{2}\rangle + 0.24 \mp\frac{11}{2}\rangle +$ $0.07 \mp\frac{7}{2}\rangle + 0.15 \mp\frac{3}{2}\rangle +$ $0.19 \mp\frac{1}{2}\rangle + 0.07 \pm\frac{1}{2}\rangle +$ $0.07 \pm\frac{3}{2}\rangle$	2.15, 3.45, 6.21	160.0	$0.1 \mp\frac{13}{2}\rangle + 0.23 \mp\frac{11}{2}\rangle +$ $0.07 \mp\frac{7}{2}\rangle + 0.14 \mp\frac{3}{2}\rangle +$ $0.18 \mp\frac{1}{2}\rangle + 0.08 \pm\frac{1}{2}\rangle +$ $0.07 \pm\frac{3}{2}\rangle$	2.84, 4.77, 6.17	163.0
294.8	$0.27 \mp\frac{11}{2}\rangle + 0.16 \mp\frac{9}{2}\rangle +$ $0.23 \mp\frac{5}{2}\rangle + 0.19 \mp\frac{3}{2}\rangle +$ $0.06 \mp\frac{1}{2}\rangle$	2.52, 1.78, 8.25	290.0	$0.23 \mp\frac{11}{2}\rangle + 0.1 \mp\frac{9}{2}\rangle +$ $0.14 \mp\frac{5}{2}\rangle + 0.15 \mp\frac{3}{2}\rangle +$ $0.1 \pm\frac{5}{2}\rangle + 0.07 \pm\frac{9}{2}\rangle +$ $0.05 \pm\frac{11}{2}\rangle$	2.39, 10.28, 3.86	286.0
327.0	$0.06 \mp\frac{13}{2}\rangle + 0.17 \mp\frac{9}{2}\rangle +$ $0.37 \mp\frac{7}{2}\rangle + 0.17 \mp\frac{5}{2}\rangle +$ $0.06 \pm\frac{9}{2}\rangle$	0.83, 6.52, 6.95	321.5	$0.06 \mp\frac{13}{2}\rangle + 0.2 \mp\frac{9}{2}\rangle +$ $0.22 \mp\frac{7}{2}\rangle + 0.11 \mp\frac{5}{2}\rangle +$ $0.07 \pm\frac{5}{2}\rangle + 0.20 \pm\frac{7}{2}\rangle$	4.90, 10.76, 3.89	322.3
358.0	$0.07 \mp\frac{13}{2}\rangle + 0.21 \mp\frac{11}{2}\rangle +$ $0.32 \mp\frac{9}{2}\rangle + 0.15 \mp\frac{7}{2}\rangle +$ $0.05 \pm\frac{5}{2}\rangle + 0.06 \pm\frac{7}{2}\rangle$	2.41, 3.57, 8.64	351.3	$0.07 \mp\frac{13}{2}\rangle + 0.12 \mp\frac{11}{2}\rangle +$ $0.25 \mp\frac{9}{2}\rangle + 0.06 \mp\frac{7}{2}\rangle +$ $0.15 \pm\frac{7}{2}\rangle + 0.10 \pm\frac{9}{2}\rangle +$ $0.10 \pm\frac{11}{2}\rangle$	10.07, 7.28, 2.73	355.2
Barycentre (\bar{E})						
169.5		165.0		165.8		

For comparison, the wave function of the ground Kramers doublet obtained using the Stevens CFPs/C_k^Q (listed in column b in Table S3) expressed in the CAS* is:

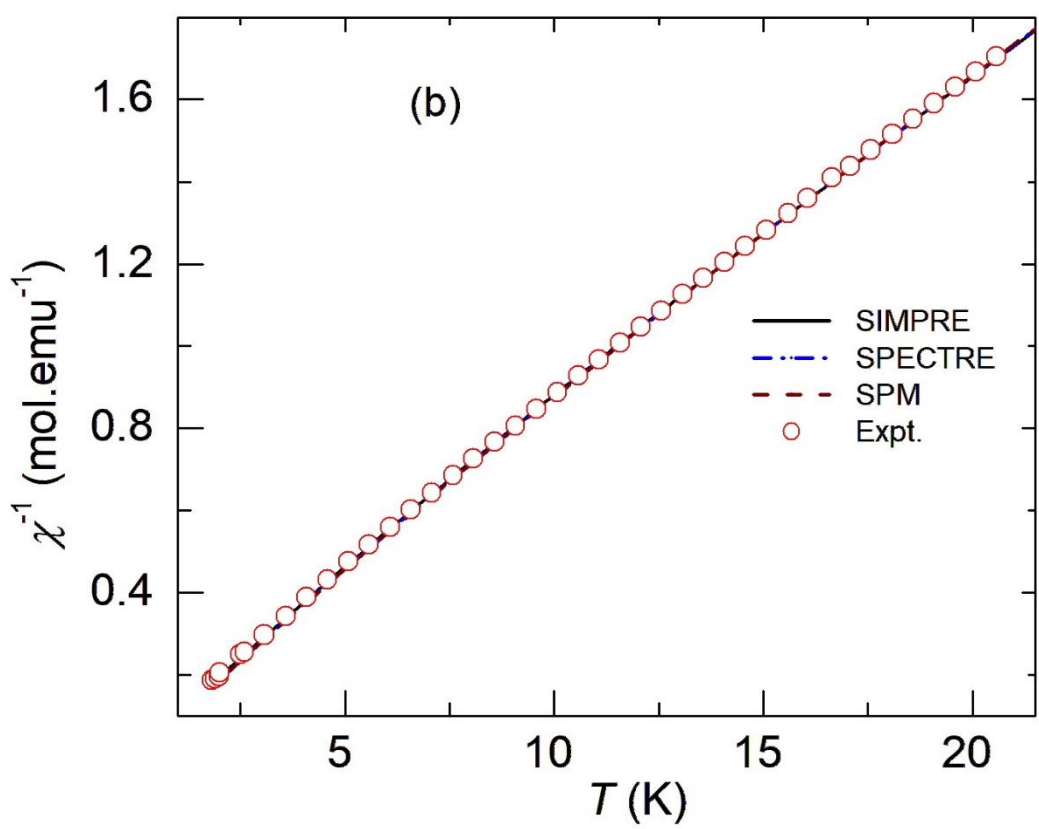
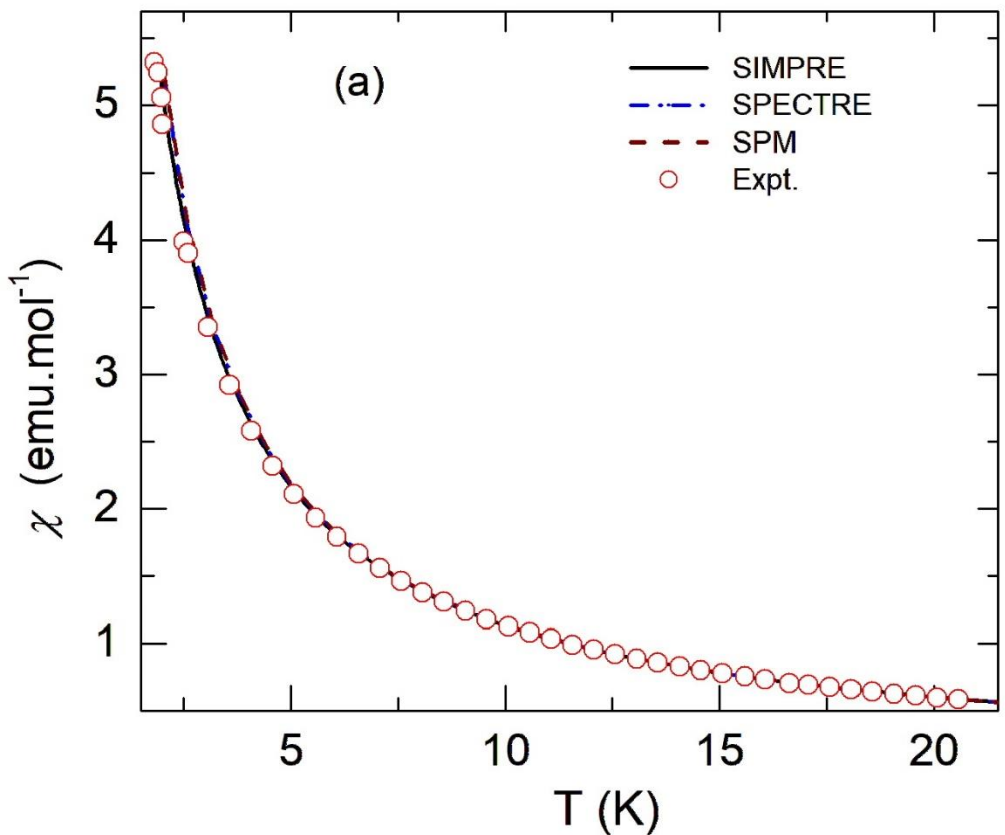
$$\Psi_0 = 0.002|\mp\frac{15}{2}\rangle + 0.05|\mp\frac{13}{2}\rangle + 0.10|\mp\frac{11}{2}\rangle + 0.17|\mp\frac{9}{2}\rangle + 0.23|\mp\frac{7}{2}\rangle + 0.20|\mp\frac{5}{2}\rangle + 0.12|\mp\frac{3}{2}\rangle + 0.024|\mp\frac{1}{2}\rangle + 0.01|\pm\frac{1}{2}\rangle + 0.014|\pm\frac{3}{2}\rangle + 0.02|\pm\frac{5}{2}\rangle + 0.005|\pm\frac{7}{2}\rangle + 0.007|\pm\frac{9}{2}\rangle + 0.03|\pm\frac{11}{2}\rangle + 0.023|\pm\frac{13}{2}\rangle + 0.003|\pm\frac{15}{2}\rangle$$

Table S5 The transition magnetic moment, $\langle\mu\rangle$ (μ_B/Dy) between the Kramers states. For explanations, see, text.

$\langle\mu\rangle$	$ +15/2\rangle$	$ -15/2\rangle$	$ +1/2, +3/2\rangle$	$ -1/2, -3/2\rangle$	$ +13/2, +5/2\rangle$	$ -13/2, -5/2\rangle$	$ +13/2, +11/2\rangle$	$ -13/2, -11/2\rangle$
$ +15/2\rangle$	3.338	0.211	1.517	0.782	1.873	0.36	0.682	0.36
$ -15/2\rangle$	0.211	3.338	0.782	1.517	0.36	1.873	0.36	0.682
$ +1/2, +3/2\rangle$	1.517	0.782	2.63	1.712	1.442	0.516	1.665	1.237
$ -1/2, -3/2\rangle$	0.782	1.517	1.712	2.63	0.515	1.442	1.238	1.666
$ +13/2, +5/2\rangle$	1.873	0.36	1.442	0.515	3.18	1.166	2.5	1.49
$ -13/2, -5/2\rangle$	0.36	1.873	0.516	1.442	1.166	3.18	1.488	2.5
$ +13/2, +11/2\rangle$	0.682	0.36	1.665	1.238	2.5	1.488	2.495	1.864
$ -13/2, -11/2\rangle$	0.36	0.682	1.237	1.666	1.49	2.5	1.864	2.495

Table S6 The percentage root-mean-square (r.m.s.) deviations, $\Delta\chi_{rms}$ ($\Delta\chi_{rms}^{-1}$), between the magnetic susceptibility χ_{ave} (inverse susceptibility χ_{ave}^{-1}) calculated using: (i) the Stevens CFPs/ C_k^q listed in column c in Table S3 calculated using RECM (computed with SIMPRE), (ii) the converted Wybourne CFPs/ B_{kq} listed in column f in Table S3 (computed with SPECTRE) and (iii) SPM CFPs/ B_{kq} given in column g in Table S3 (computed with SPECTRE), and the experimental data.² For explanations, see, text.

	$\Delta\chi_{rms}\%$			$\Delta\chi_{rms}^{-1}\%$		
	1.8 – 300 K	1.8 – 20 K	200 – 300 K	1.8 – 300 K	1.8 – 20 K	200 – 300 K
RECM/ SIMPRE	0.2	0.47	0.08	0.03	0.08	0.08
RECM/ SPECTRE	0.34	0.83	0.2	0.1	0.12	0.22
SPM/ SPECTRE	0.35	0.9	0.2	0.1	0.14	0.23



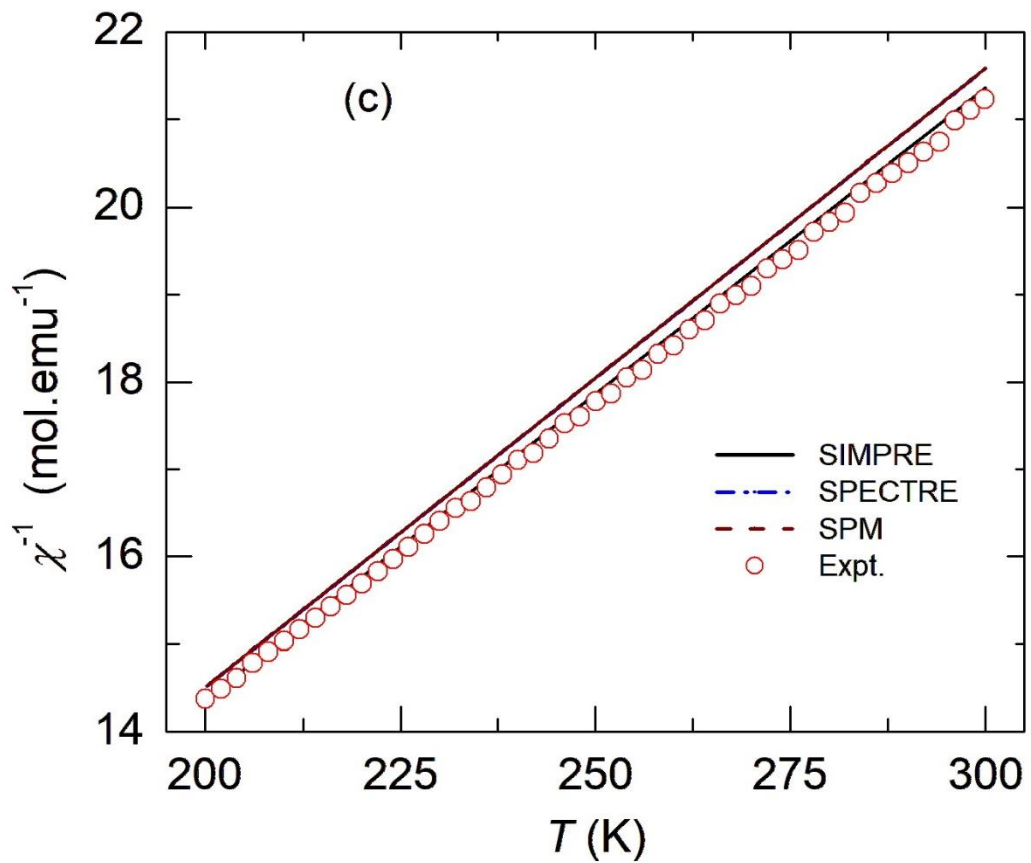


Fig. S2 Temperature variation of the dc magnetic susceptibility: (a) χ within 1.8–20 K, (b) χ^{-1} within 1.8–20 K, and (c) χ^{-1} within 200–300 K predicted using: (i) the Stevens CFPs/ C_k^q listed in column c in Table S3 calculated using RECM (computed with SIMPRE), (ii) the converted Wybourne CFPs/ B_{kq} listed in column f in Table S3 (computed with SPECTRE) and (iii) SPM CFPs/ B_{kq} listed in column f in Table S3 (computed with SPECTRE), and the experimental data (\circ).² For explanations, see, text.

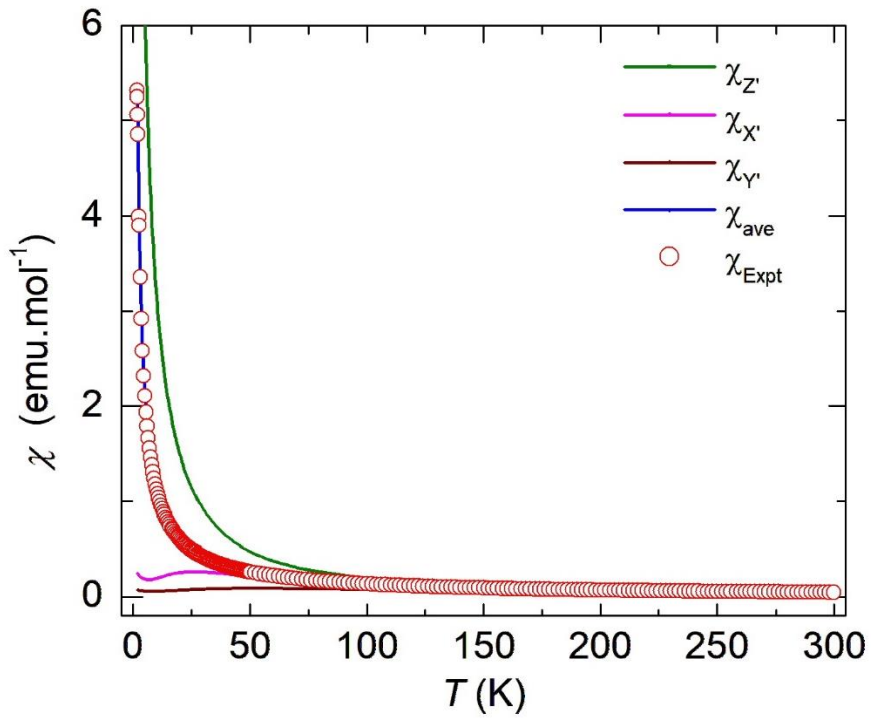


Fig. S3 Temperature variation of the directional magnetic susceptibility along the (X' , Y' , Z') axis of the rotated CAS* system computed with SIMPRE using the Stevens CFPs/ C_k^q (listed in column c in Table S3) together with the calculated average susceptibility χ_{ave} that matches with the experimental data (\circ) recorded at $H = 0.1$ T.²

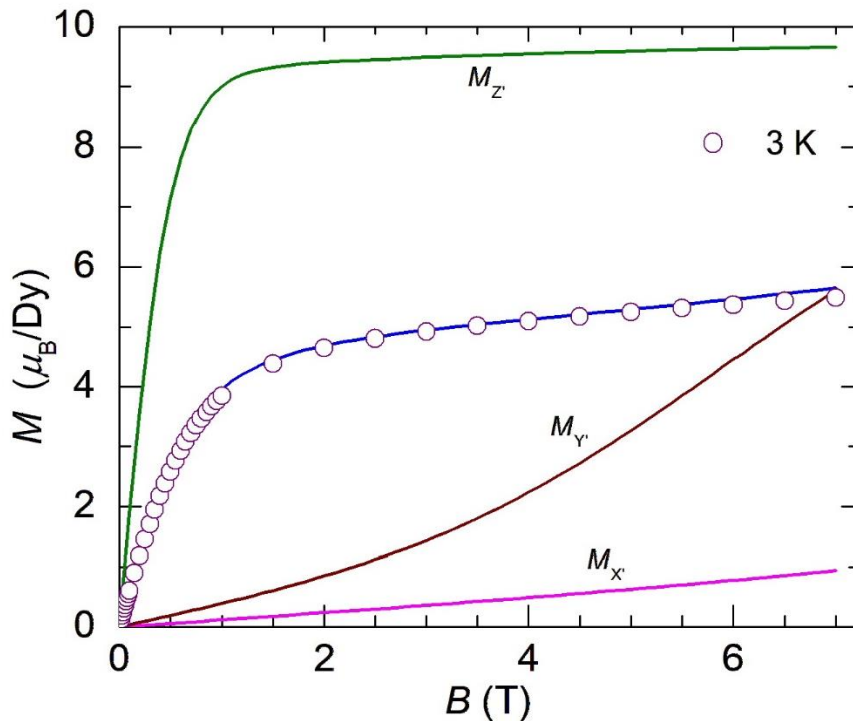


Fig. S4 Directional magnetization along the (X' , Y' , Z') axis of the rotated CAS* system predicted at $T = 3$ K using the Stevens CFPs/ C_k^q (listed in column c in Table S3) with the calculated average of magnetization M_{ave} (blue line) that matches with the experimental data (\circ) at $T = 3$ K.²

References

- 1 B. Devi, R. R. Koner and A. Halder, *New J. Chem.*, 2017, **41**, 7972–7979.
- 2 S. Singh, Sheetal, B. Devi, R. R. Koner, A. Halder and C. S. Yadav, *EPL*, 2020, **130**, 47002.